Benchmarking the Multipass Beam-Breakup Simulation Code BI

OAG-TN-2008-029

Aminur Rahman – 8/12/2008

Department of Mathematical Sciences
New Jersey Institute of Technology
Newark, New Jersey 07102-1982
ar276@njit.edu

Nicholas S. Sereno and Hairong Shang

Accelerator Systems Division, Advanced Photon Source

Abstract

Multipass beam-breakup (BBU) is a potentially serious performance limiting instability that can arise in recirculating or energy-recovery linacs (ERLs) if not understood and carefully controlled. The instability is driven by parasitic higher-order modes (HOMS) that kick the beam transversely (or longitudinally) on low energy passes. The beam can arrive displaced on subsequent passes and coherently drive the same modes that produced the kicks setting up a potentially unstable feedback loop. If the average beam current is above the threshold for the instability, the beam displacements from HOM kicks grow exponentially and the beam is quickly lost. The APS 7 GeV ERL concept [1] requires up to 100 mA average which to this date is about an order of magnitude higher than has been achieved in present-day ERLs.

Beam Instability (BI) [2] by Ivan Bazarov, is a beam breakup (BBU) code which we use to simulate transverse BBU for the APS 7 GeV ERL. We first benchmark the code against simple analytical formulas where the threshold current is calculated from first principles independently. After benchmarking, BI will be used to do threshold current calculations for the APS 7 GeV ERL latice for multiple HOMs per cavity and various HOM frequency distributions. The calculations will determine how much the HOMs need to be detuned from cavity to cavity to give threshold currents comfortably above 100 mA. In this paper we describe the benchmarking process and simulations for the full 7 GeV ERL concept.

1 Introduction: Energy Recovery Linacs and Beam Breakup

1.1 Energy Recovery Linacs

Light source applications of ERLs are presently being investigated by a number of laboratories due to the low beam emittance and high average current that can be accelerated by the device [1, 3, 4]. High average current is achieved in ERLs because the beam kinetic energy is returned to the accelerating mode of the superconducting cavities after the beam has been used to produce light (from infared to X-rays). One can think of an ERL as a particle accelerator analogy of a hybrid car. In a hybrid car the battery is discharged when accelerating, and recharged during deceleration. This way some of the energy is recovered. In the case of an ERL, the accelearating beam takes energy from the cavity field and gains kinetic energy. When the beam is decelerating (180 degrees out of phase with the accelerating beam) the beam returns some of its kinetic energy to the cavity field. When the beam gets to the end of the linac, it can in principle return all of its kinetic energy back to the cavity fields. In a single-pass linac the beam would simply get dumped after producing light. The beam power at the dump can be as high as 700 MW (100 mA at 7 GeV) making operation of the linac far too costly in terms of electric power required not to mention the radiation hazard present at the beam dump. The superconducting cavities allow efficient acceleration and energy recovery in an ERL due to their extremely low wall losses.

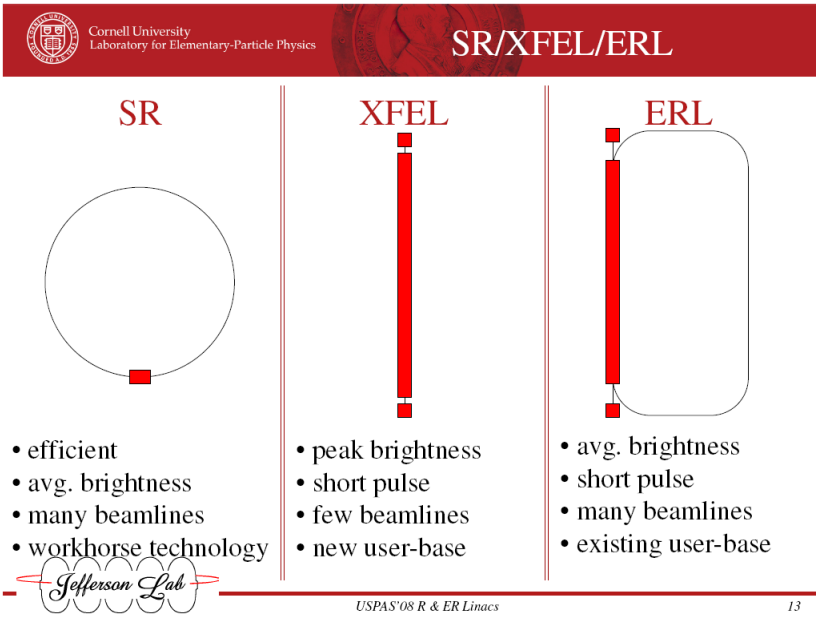

Figure 1: Comparison of SR, XFEL, and ERL light sources [5]

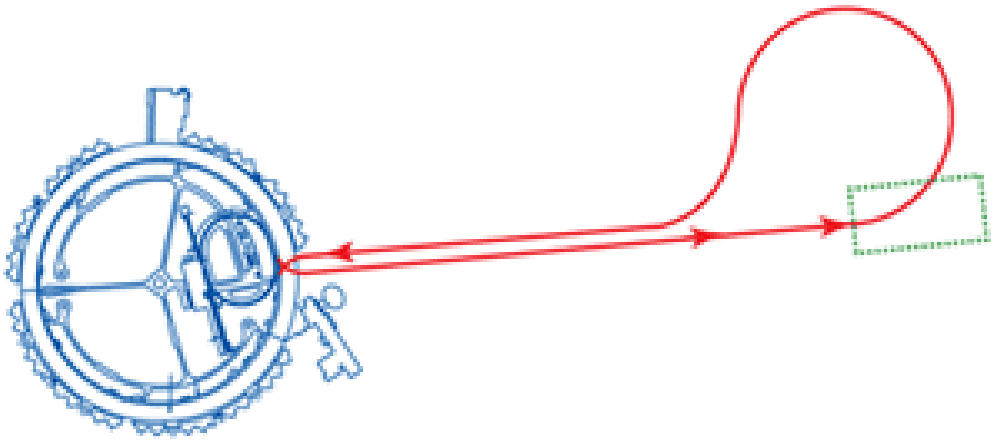

Figure 2: APS 7GeV ERL concept [1]

Figure 1 shows a brief comparison between storage ring, X-ray FEL and ERL light sources. At present, the APS uses a linac, accumulator ring and booster as an injector to fill the storage ring and circulate beam for many hours in top-up mode. Figure 2 shows the APS 7 GeV ERL concept [1]. The present APS storage ring will be used as part of the recirculation arc of the ERL. In addition, a large turn-around arc will be used to expand the user base by offering long straight sections. The linac accelerates the beam away from the APS toward the large turn-around arc. The beam is then brought back to the APS ring and circulated around the ring. Finally, the beam energy is recovered on the second pass through the linac.

1.2 Multipass Beam Breakup

The multipass BBU instability is due to the interaction of HOMs with the beam under conditions where the beam is recirculated. Above a certain current known as the threshold current, the HOM fields become larger as time passes until they eventually kick the beam out of the machine possibly causing severe damage to expensive hardware. It is therefore important to understand what HOM and linac parameters determine the value of the threshold current. It is desireable for the threshold current be well above the design current of the ERL or recirculating current by at least an order of magnitude. This is because the threshold current depends sensitively on HOM and linac optical parameters as we will investigate by means of the simplest example of a recirculating linac-namely a linac consisting of a single cavity, single HOM and one recirculation. In what follows we analyze this simple example and use it to benchmark the code BI which will be used to simulate beam breakup in real linac with many cavities with multiple HOMs.

2 Analysis of Single Cavity, Single HOM, Single Recirculation Linac

Figure 3 shows the simple system analyzed in detail previously [6, 7, 8, 9, 10]. The beam enters the cavity on the first pass with momentum p_i. The beam receives a transverse kick at the cavity by the HOM and is recirculated back to the cavity on the second pass with displacement given by.

$$x_c^{(2)}(t) = M_{12}^{(r)}\theta_c^{(1)}(t - t_r), \tag{1}$$

where $M_{12}^{(r)}$ is the matrix element that determines how much displacement results from an upstream kick. Since the transverse cavity HOMs are TM11 modes, they have a non-zero electric field only off axis. This means that if $M_{12}^{(r)}$ is zero, the HOM field cannot grow due to the kick given the beam on the first pass. Within the limits of this simple example, if $M_{12}^{(r)}$ is zero the threshold current would be infinite since the HOM cannot drive itself through the feedback mechanism provided by beam recirculation.

In general, we can define a potential function called the wake potential which is proportional to the transverse momentum kick the HOM (magnetic) field gives the beam according to

$$p_x(t) = \frac{eV(t)}{c}. \tag{2}$$

The angular kick is given in terms of the wake potential according to

$$\theta_c^{(1)}(t) = \frac{p_x(t)}{p_r}. \tag{3}$$

where p_r is the momentum of the recirculated beam. The wake potential function ultimately depends on the value of the electric and magnetic fields of the HOM at any given instant in time. It therefore depends on the contributions to the field from the beam that has passed displaced through the cavity. The wake potential can be written,

$$V(t) = \int_{-\infty}^{t} W(t - t')I(t')x_c^{(2)}(t')dt' \tag{4}$$

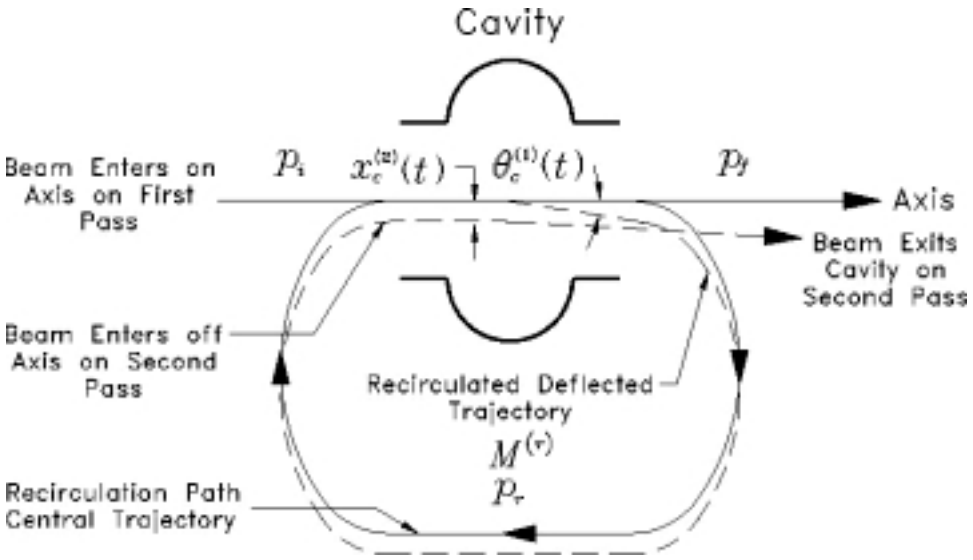

Figure 3: Single cavity linac with a single recirculation path. the cavity is assumed to contain a single HOM in addition to the fundamental acceleration mode.

where $I(t)$ is the beam current which is modelled as a series of delta function pulses and $W(\tau)$ is the wake function. The wake function quantifies how much a given charge called the "exciting charge" (which excites the HOM field) passing displaced through a cavity HOM field kicks a test charge following behind. It therefore acts as a greens function in the integral equation for the wake potential. The integral equation adds up all the contributions to the HOM fields (and hence kick) at a given time from all the beam bunches that have passed the cavity displaced on the second pass. Substituting $x_c^{(2)}(t)$ into the integral equation results in

$$V(t) = \frac{eM_{12}^{(r)}}{p_r c} \int_{-\infty}^{t} W(t-t')I(t')V(t'-t_r)dt' \tag{5}$$

where the wake potential depends on itself delayed by the recirculation time. Equation says that the wake potential at a given time depends on its value at all previous time since beam has been in the cavity. Another way this equation can be written is

$$x_c^{(2)}(t) = \frac{eM_{12}^{(r)}}{p_r c} \int_{-\infty}^{t-t_r} x_c^{(2)}(t')W(t-t_r-t')I(t')dt' \tag{6}$$

This equation shows that the displacement of the beam at time t is due to all the displacements of previous bunches from the time the beam was on. This is again because the only way the HOM can feedback energy to itself through the beam is when the beam passes off axis where the HOM electric field is non-zero. Since the HOM fields oscillate periodically in time, the equation for the wake potential can be solved assuming a normal mode solution.

$$V(t) = V_\circ e^{i\omega t} \tag{7}$$

This has been done previously [6] and an approximate equation for the threshold current can be derived assuming Im(ω) is zero. The formula is

$$I_{th} = \frac{-2p_r c}{e(R/Q)_m Q_m k_m M_{12}^{(r)} \sin(\omega_m t_r)}. \tag{8}$$

This formula shows how the threshold current depends on the various parameters. As discussed previously, if $M_{12}^{(r)}$ is zero, the threshold current within the bounds of this simple example is infinte

since the second pass displacement of the beam is always zero. The momentum dependence is due to the fact that it is harder to kick a high momentm beam. One therefore expects the threshold current to be larger if the beam momentum is higher. The threshold current goes down the larger $(R/Q)_m$ becomes since this quantity determines how well a displaced beam couples to the HOM. Similarly, if Q_m of the HOM is large, it takes longer for the HOM to dissapate energy put into it by the beam which also results in a lower threshold current. The phase factor in the denominator is due to the fact the amount of energy the beam can put into the HOM depends the orientation of the HOM electric field which depends on how long it takes for the beam to recirculate from first to second pass. Finally, in terms of energy exchange, the threshold current is the average beam current where the energy given up by the beam to the HOM fields equals the energy dissipated by the HOM due to losses.

Equation 8 is an approximate solution to an exact equation derived from assuming a normal mode solution for the wake potential in equation 5 (or equivalently the position of the beam in equation 6). The exact equation is,

$$\begin{aligned} 1 &= \kappa e^{i\omega t_r}\left\{\frac{\xi\sin(\omega_m t_\circ)}{1-2\xi\cos(\omega_m t_\circ)+\xi^2}\right\} \\ \xi &= e^{-\frac{\omega_m t_\circ}{2Q_m}}e^{i\omega t_\circ}. \\ \kappa &= \frac{eM_{12}^{(r)}I_\circ t_\circ (R/Q)_m k_m \omega_m}{2p_r c}, \end{aligned} \tag{9}$$

where we can consider this an equation either with ω complex or $I_\circ$ complex. It is more straightforward to consider the latter and keep ω real and search for values of ω where $I_\circ$ is real. The smallest positive real current will be the threshold. In general there are an infinite number of frequencies where $I_\circ$ is real due to the trigonometric nature of equation 9. A script was written to search for values where the complex current is purely real. The search is centered about the HOM frequency since that is where we know the beam-HOM system will oscillate. The script was used to benchmark the beam instability code BI.

3 Overview of the Beam Instability code

The BI code simulates multipass beam break up. It can search for the threshold current by iteratively determining when the beam is stable by varying the current until sufficient accuracy is obtained. The code also outputs, in tabular form, the position of the centroid and the voltage of the beam with respect to time, for both x and y directions at the position of the rf cavities. The input data is provided in three files. One file contains, in tabular form, the HOM parameters $(R/Q)_m$, Q_m ω_m and the polarization angle θ_m. Another file contains the, current, time the beam is on, print interval time, bunch frequency, and injection energy. The last file has the usual 6x6 transport matrix for each element of the linac as well as the recirculation arc. The code is invoked from the commandline. The threshold current output goes to stdout and the coordinate data is written to a file. Various scripts were written to translate this output into sdds for postprocessing using the toolkit [11].

4 Benchmarking the BI Code

Equation 9 was solved numerically for a typical HOM parameters for a 7-cell cavity design anticipated for use in the Cornell ERL and compared to the output of BI. The 7-cell HOM parameters were used to compute the threshold current assuming $M_{12}^{(r)} = -8$ m. Table 1 lists the HOM parameters used in the benchmarking. This particular HOM had relatively large $(R/Q)_m$ and Q_m compared to the other HOMs.

Figure 4 shows the plot of real current versus imaginary current calculated numerically by separating equation 9 into real and imaginary parts. The smallest positive real value of the current when the imaginary value is zero is the threshold current. Table 2 shows the comparison of threshold

f_m	Q_m	$(R/Q)_m$
1.87394 GHz	20912.4	109.60Ω

Table 1: One of the dominant transverse HOMs for the Cornell 7-cell ERL cavity [12].

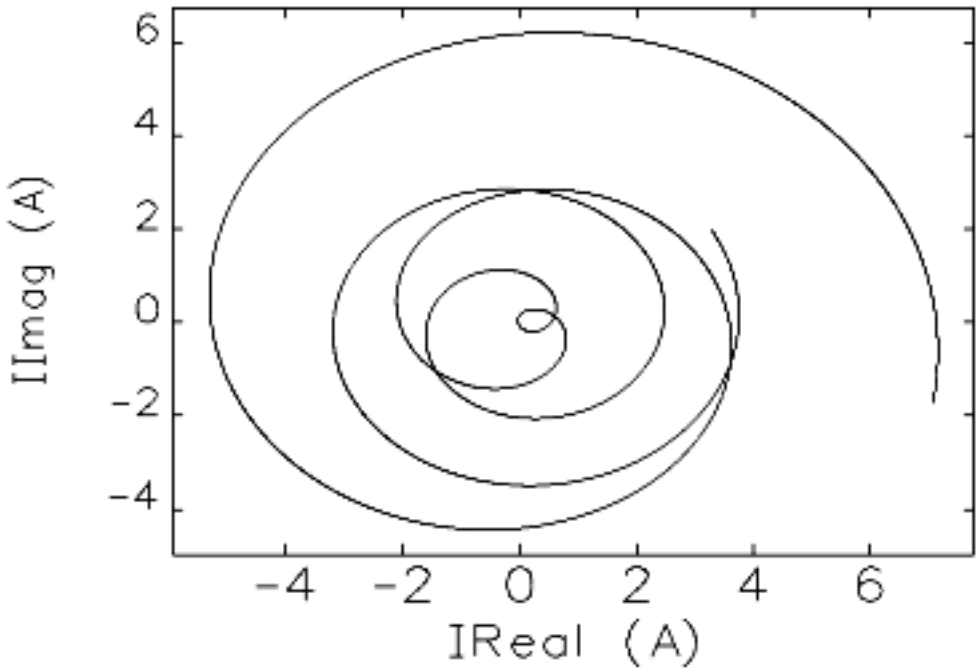

Figure 4: Plot of the real current versus the imaginary current

	frequency	threshold current
Analytical Formula	1.87394 GHz	0.0384 Amperes
BI	1.87409 GHz	0.0386 Amperes

	frequency	threshold current
Analytical Fromula	1.873 GHz	0.0655 Amperes
BI	1.873 GHz	0.3632 Amperes

Table 2: Comparison of threshold current calculated from BI and the analytic formula given by equation 9. The top table shows the two agree if the frequency is adjusted slightly. The bottom table shows how different the thresholds can be if the HOM frequency adjustment is not made.

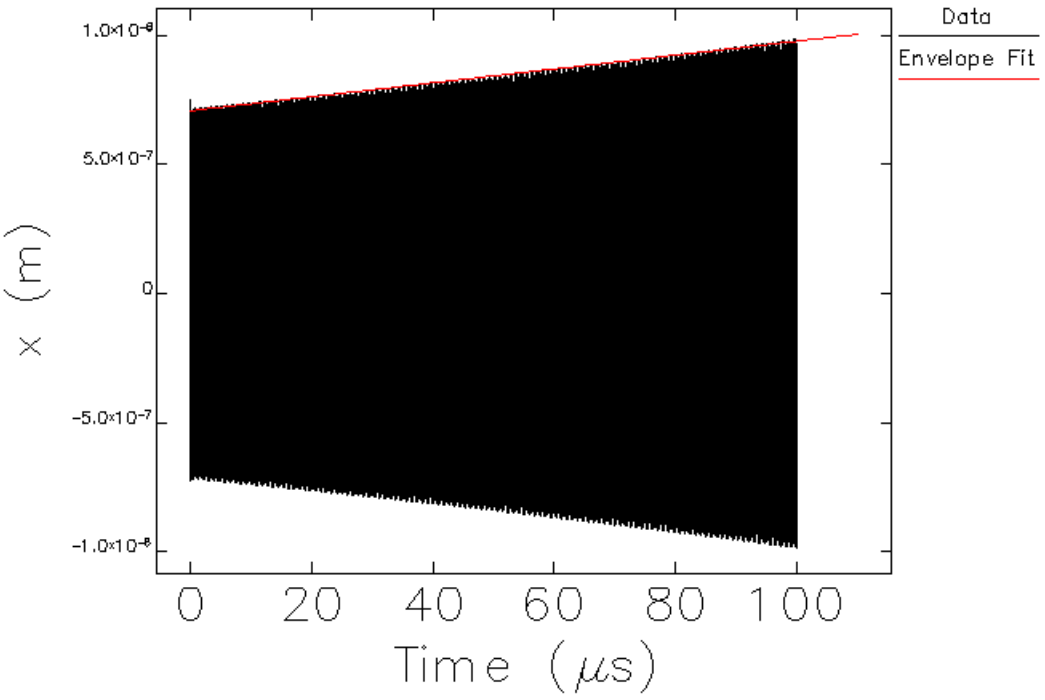

Figure 5: Plot of the displacement in the x direction versus time.

current calculated from BI and the analytic formula given by equation 9. The top table shows the two agree if the frequency is adjusted slightly. The bottom table shows how different the thresholds can be if the HOM frequency adjustment is not made. The comparison in the tables shows that the threshold current can depend very sensitively on the HOM and lattice parameters. The sensitivity is indicated in equation 8 because the phase factor in the denomintor $\sin(\omega_m t_r)$ can be zero or close to zero by a small change in frequency. The BI code and numerical calculation can be affected by differences in round-off error or even how the momentum depending on whether the electrons are assumed to move at the speed of light or slight corrections are made for the fact that the electrons actually move somewhat less than c. One sees from table 2 that changing the HOM frequency by only 0.008% results in a change in the threshold current by a factor of 10. Tests were done for modes vertically polarized for $M_{34}^{(r)} = -8$ m which achieved similar benchmarking results to those in table 2.

Another benchmarking test is to see how the threshold current computed using BI compares to the analytic formula for a HOM polarization angle of 30°. For this test we are required to use the "effective matrix element" M^* in place of $M_{12}^{(r)}$ for the numerical computation because our analytical formula only applies to the case of either the horizontal or vertical plane. Both BI and the analytic formula should give the same threshold current since for linear optics, there is no preferred HOM polarization plane. The equation for the effective matrix element is given by [12].

$$M^* = M_{12}^{(r)} \cos^2(\theta_m) + \frac{M_{14}^{(r)} + M_{32}^{(r)}}{2} + M_{34}^{(r)} \sin^2(\theta_m). \tag{10}$$

For our matrix $M_{14}^{(r)}$ and $M_{32}^{(r)}$ both equal to zero so the equation reduces to:

$$M^* = M_{12}^{(r)} \cos^2(\theta_m) + M_{34}^{(r)} \sin^2(\theta_m). \tag{11}$$

	frequency	threshold current
Analytical Fromula	1.8744 GHz	.0404 Amperes
BI	1.8744 GHz	.0397 Amperes

Table 3: Threshold current comparison for 30° HOM polarization

where $M_{12}^{(r)} = M_{34}^{(r)} = -8$ m and $\theta_m = 30°$. After plugging the values in we get $M^* = -8$ m. Next we run BI and see that the result matches to within 1.6% of analytical formula as shown in table 3. For final benchmarking we calculate the growth rate using BI and compare it to the analytical formula,

$$\tau = \frac{2Q_m}{\omega_m} \times \frac{I_{th}}{\delta I_\circ} \tag{12}$$

derived from equation 2.40 [7] under the approximation that the growth time is large compared to the HOM period. To calculate the growth rate from BI we fit the envelope of the horizontal position at the cavity to the equation,

$$x(t)_{\text{env}} = Ae^{\frac{t}{\tau}} \approx A\left(1 + \frac{t}{\tau}\right) \tag{13}$$

where A is the amplitude at the beginning of the simulation and τ is the growth time. Figure 5 shows the results. The slope of the line is given by $m = \frac{A}{\tau} \Rightarrow \tau = \frac{A}{m}$. For this simulation, we used $I_\circ \approx 1.02 \times I_{th}$. From figure 5 we obtain $\tau = 263.3$ μs using BI compared to $\tau = 312.7$ μs using the analytical formula given by equation 12. This indicates agreement to within 16% which is good for this benchmarking test.

5 Concluding Remarks

Benchmarking the code was a success and we know that the code works. However, we were not able to get believable results for the full 7 GeV linac simulations. We will continue work on the script that converts the ERL lattice to BI input and do more tests to find out how it needs to be modified to get results that can be trusted. We anticipate this is simply a matter of investigating how the code BI uses the HOM parameters and 6x6 input matrix. Simulations of multipass BBU of the full 7 GeV APS ERL design will be performed in subsequent work after full debugging of the scripts that prepare input to BI.

6 Acknowledgement

The authors wish to thank the administrators and mentors of the Lee Teng internship program at Argonne for their support of this work. Thanks to R. Soliday for maintaining the “weed” computing cluster used for the benchmark simulations.

References

[1] M. Borland, G. Decker, A. Nassiri, Yin-e Sun, M. White, Potential performance and challenges of an energy recovery linear upgrade to the Advanced Photon Source, ”NIM A”, 582, ”54-56”, 2007

[2] I.V. Bazarov, BI Version 0.7 (2005).

[3] ”Energy Recovery Linac Project at Cornell University”, Journal of Synchrotron Radiation, Vol. 10, Part 5 (2003) 346-8

[4] D. Douglas “The Jefferson Lab 1 KW IR FEL,” Proceedings of the 2000 linear accelerator conference, pp 716-720, (2000).

[5] I.V. Bazarov and G. Krafft, Recirculated and Energy Recovery Linacs, United States Particle Accelerator School (Winter 2008).

[6] G. A. Krafft, J. J. Bisognano, S. Laubach, "Beam Breakup in Superconducting Linacs, CEBAF Technical Note unpublished, 1990.

[7] N.S.R. Sereno, Experimental Studies of Multipass Beam Breakup and Energy Recovery Using the CEBAF Injector Linac, Doctoral Thesis: University of Illinois at Urbana-Champaign (1994).

[8] G.H. Hoffstaetter and I.V. Bazarov, Beam-breakup Instability Theory for Energy Recovery Linacs, PRST-AB, **7**, 054401, (2004).

[9] G.H. Hoffstaetter, I.V. Bazarov, and C. Song, Recirculating Beam-breakup Thresholds for Polarized Higher-Order Modes with Optical Coupling, PRST-AB, **10**, 044401, (2007).

[10] E. Pozdeyev, Regenerative Multipass Beam Breakup in Two Dimensions, PRST-AB, **8**, 054401, (2005).

[11] M. Borland, L. Emery, and H. Shang, R. Soliday, SDDS Toolkit Version 1.30 (2008).

[12] C. Song and G. Hoffstaetter, Beam Breakup Simulations for the Cornell X-Ray ERL, (2007 or 2008).